JOURNAL OF THE GEOTECHNICAL ENGINEERING DIVISION

ENERGY DYNAMICS OF SPT

By John H. Schmertmann,[1] F. ASCE
and Alejandro Palacios,[2] M. ASCE

INTRODUCTION

The standard penetration test (SPT) hammer falls, strikes the rods, and in only milliseconds produces a part of the final SPT sample and blow count. The writers herein explore this dynamic event in detail.

The research that provides the basis for this paper began with a study of the quasi statics of the SPT (12,14). The research then continued with the use of dynamic load cells placed in the string of SPT rods, at first just below the hammer and later just above the sampler. The second writer (11) then searched for and found a theory that seemd to provide a basis for understanding the load-cell data. This theory also led to a method for measuring some of the energy transfers that occur during the SPT. More tests confirmed the theory and demonstrated the commanding importance of the energy content of the first compression wave entering the rods. Finally, wave equation modeling on a computer permitted a detailed examination of the SPT sampling process.

ENERGY THEORY

Energy Transfer from Hammer to Rods.—Fairhurst (3) describes what ideally happens when two similar materials impact. A compression wave travels with the same velocity both down the rods and up the hammer. Because of the relatively short length of the hammer, the compression wave reaches the end of the hammer relatively quickly. On reaching the free, tip end of the hammer this wave reflects in the hammer as a tension wave of the same magnitude and form. This tension wave then progressively erases the continuing, up-coming compression wave until finally the hammer carries no stress when the tension

Note.—Discussion open until January 1, 1980. To extend the closing date one month, a written request must be filed with the Editor of Technical Publications, ASCE. This paper is part of the copyrighted Journal of the Geotechnical Engineering Division, Proceedings of the American Society of Civil Engineers, Vol. 105, No. GT8, August, 1979. Manuscript was submitted for review for possible publication on October 24, 1978.

[1]Principal, Schmertmann & Crapps, Inc.; Prof. of Civ. Engrg., Univ. of Florida, Gainesville, Fla.

[2]Consulting Engr., CESCO, Cali, Colombia.

wave returns to the point of hammer contact. However, the rods still remain in contact with the hammer because they still carry a compressive wave stress. Then a new, again reflected hammer compression wave begins at the contact and puts a new pulse, at a reduced stress and energy level, into the rods. This process continues with each cycle of wave transmission and reflection in the hammer, producing a progressively stepped, reduced level of compressive stress in the compression wave originating at the contact and traveling down the rods.

The shape of the force-time wave that initially travels down the rods depends primarily on the hammer-rod impedance ratio r. For hammer and rods of the same material, r equals the ratio of the cross-sectional area of the rods a to the area of the hammer A_h, or

$$r = \frac{a}{A_h} \quad \ldots\ldots (1)$$

As explained previously, each cycle of the wave in the hammer produces a successively reduced magnitude of stress in the rods. The first cycle has the greatest stress magnitude σ_{max} given by Fairhurst (3) as

$$\sigma_{max} = \rho c \left(\frac{V_{hi}}{1+r}\right) \quad \ldots\ldots (2)$$

in which ρ = mass density of material; c = velocity of compression wave in rods; and V_{hi} = velocity of hammer at impact. For the nth cycle

$$\sigma = \sigma_{max}\left(\frac{1-r}{1+r}\right)^n \quad \ldots\ldots (3)$$

The writers (Ref. 11, Fig. 3.5 and Ref. 15, Fig. 9) have illustrated the theoretical stepdown of stress delivered to the rods for four hammer-rod impedance ratios while keeping the same hammer weight of 140 lb (620 N). The shorter the SPT hammer, the higher the magnitude of peak stress and the smoother the stress wave form. Eq. 4, from Fairhurst (3), expresses the limiting continuously decaying (infinite number of steps) stress wave form for the rigid hammer case when $r = 0$

$$\sigma = \rho c V_{hi} \exp\left(-\frac{a\rho c}{m} t\right) \quad \ldots\ldots (4)$$

in which m = the mass of the hammer; t = time from impact; and a = the rod area.

Fairhurst (3) showed five examples of excellent agreement between experimental stress wave forms and those determined from the preceding theory. The writers offer Fig. 1 as a typical check of theory against an actual experimental SPT wave form. These and many other examples by a variety of investigators confirm the preceding as an accurate theory for the hammer-rod impact problem.

The hammer and rods only remain in contact until the tension cutoff shown in Fig. 1. The initial compression wave in the rods reflects at the sampler end of any real SPT rod system with finite length and returns as a tension wave. When this tension wave reaches the hammer-rod contact point its tension

stress magnitude exceeds the then existing contact compressive stress between the hammer and rods. This produces a net tensile stress and strain that causes the rods to pull down and away from the hammer.

The preceding tension cutoff effectively stops further transfer of energy from hammer to rods. The hammer will eventually again make contact with the rods, producing a "second impact." However, the SPT sampler penetration occurs so rapidly, with 90% in less than 50 msec (as considered subsequently), that the second and any subsequent impacts occur too late to increase penetration significantly.

The preceding assumes that the initial compression wave will not reflect as another compression wave, which can happen with sufficient end restraint at the sampler. However, in this research, to N and $N' = 50$ the writers observed only reflected tension waves of sufficient magnitude to produce a net tension at the hammer.

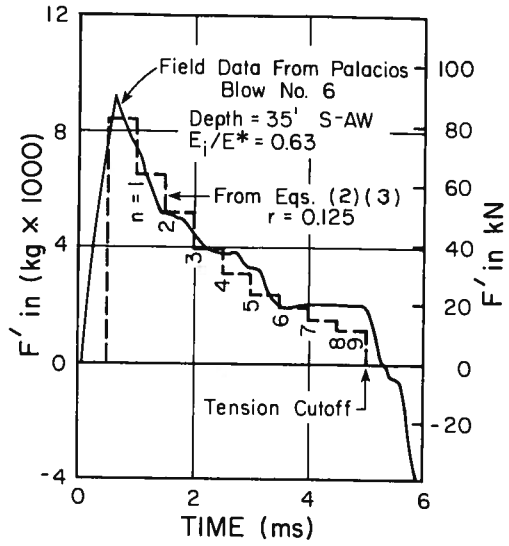

FIG. 1.—Check of Theoretical Wave Form Against Field Data

Energy Content of First Compression Wave in Rods.—A compression wave traveling down a cylindrical rod carries a fixed amount of energy. Mechanics theory (4,8) shows that in linearly elastic materials the total energy in a single wave divides equally between kinetic energy contained in the movement of the rod particles and compression energy stored by the spring action of the rod. Eq. 5 gives the total energy in a compression wave passing a point during any time interval. One can easily convert stresses in the rods to forces by noting that force equals stress divided by area, giving Eq. 6. Thus, to determine the energy in the first compression wave passing a point during any time interval one need only square the force and integrate the thus modified force-time relationship during this time interval. A squared force means: (1) That the peak force portion of a wave dominates the energy contained; and (2) after squaring

either a negative tension or positive compression force one obtains a positi energy content, i.e.

$$E = E_{potential}(50\%) + E_{kinetic}(50\%) = \frac{a\,c}{M}\int_{t_1}^{t_2}\sigma^2\,dt \quad \ldots\ldots\ldots\ldots\ldots (5)$$

$$E = E_{potential}(50\%) + E_{kinetic}(50\%) = \frac{c}{a\,M}\int_{t_1}^{t_2}F^2\,dt \quad \ldots\ldots\ldots\ldots\ldots (6)$$

in which E = energy in rods; a = area of rod cross section; c = velocity of compression wave in rods; M = Young's modulus of rods; σ = normal stress in rods; F = normal force in rods; and t = time from hammer impact.

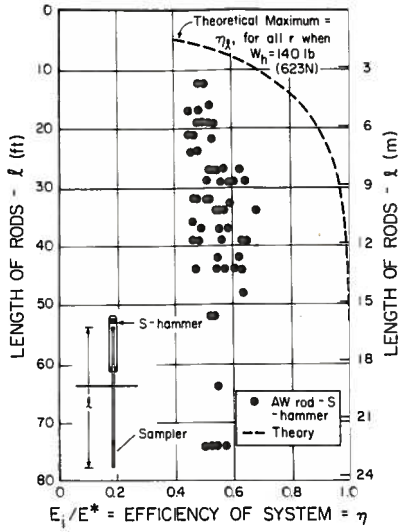

FIG. 2.—Theoretical Maximum and Measured Efficiencies of Hammer Energy Delivered to Rods in First Compression Wave

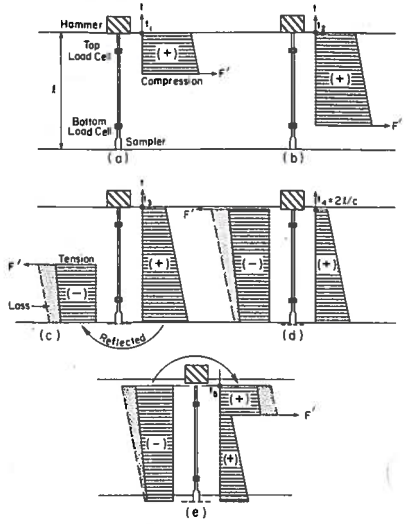

FIG. 3.—Schematic of First Compression Wave Reflecting at Sampler and Then at Hammer

Tension Cutoff of Hammer Energy.—The tension cutoff of the hammer energy input to the rods occurs at time $2l/c$, in which l = the length of the SPT rod and sampler system. The compression wave stops abruptly and loses that part of the hammer energy that would otherwise transfer to the rods between $t = 2l/c$ and t = infinity. Eq. 7, modified from Fairhurst (3) by the second writer (11), expresses a hammer energy transfer efficiency factor η_l due only to the finite length l of the rods, i.e.

$$\eta_l = (1 - K^{n'}) + \left(\frac{l}{L_h} - n'\right)\frac{4rK^{n'}}{(1+r)^2} \quad \ldots\ldots\ldots\ldots\ldots\ldots (7)$$

in which $K = [(1 - r)/(1 + r)]^2$; n' = maximum number of completed stress steps before loss of hammer contact; and L_h = the length of the hammer.

Note that $l/L_h > n' > [(l/L_h) - 1]$. The dashed line in Fig. 2 presents the results of using Eq. 7 with the 140-lb (620-N) steel SPT hammer and AW rods. Test calculations have shown that for a given hammer weight, η_l remains almost independent of L_h and r.

The η_l line in Fig. 2 shows the maximum percentage of the kinetic energy in the hammer that could possibly enter the rods before the tension wave cutoff. Note that η_l reaches practically 1.0 for l = 40 ft (12 m) or longer.

How Sampler Accepts Energy for Sampling.—Fig. 3 shows a schematic sequence of the hammer-impact wave pulse moving up and down the rods and through the two load cells mentioned previously. In this sequence, the writers have simplified the shape of the stress or force wave form. Fig. 3(*a*) shows the wave peak past the top load cell, but not yet to the bottom cell at time t_1 since hammer impact. Fig. 3(*b*) shows the peak just at the bottom cell at the later time t_2. The sampler does not yet know the hammer has struck. Fig. 3(*c*) at time t_3 shows that the front of the wave form has reflected as a tension wave, which then returns up the rods. Now the sampler has felt the blow and has started its penetration against soil resistance. It therefore takes energy out of the wave and reduces its stress or force amplitude—shown by the shading. The bottom cell now records the sum of the still-arriving tail of the compression wave and the head of the reflected tension wave. Fig. 3(*d*) shows the tension wave past the top load cell and just arriving at the hammer at time t_4 since impact. At this time the rods pull away from the hammer and it stops its energy transfer to the rods. The tension wave then reflects at the now free hammer end of the rods and moves back down the rods as a second cycle compression wave. Fig. 3(*e*) at time t_5 shows this second compression wave past the top cell and on its way down to the bottom cell to energize a possible second increment of sampler penetration. These wave traverses continue until the force magnitude of the last compression wave can no longer induce further sampler penetration, and the remaining wave energy dissipates uselessly.

Energy Measurements

Use of Load Cells.—To obtain the wave energy passing any point in the rods during a specified time interval, Eq. 6 shows that one need know only some constants and the force-time wave form during that interval. As noted previously, the writers had two load cells available to measure the force-time wave forms and thus to measure passing wave energy. Refs. 11 and 13 show photos of the load cells. The following further describes these cells and their use.

The writers had these strain-gage load cells built suitable for screwing directly into the string of SPT rods and for insertion into a wet borehole. These cells also had hollow centers to match, approximately, the inside diameters of the rods used. Both cells had a length of 6 in. (150 mm) and an effective spring constant stiffness of approx 0.7 that of an equal length of rod. Subsequent detailed wave equation studies by Gallet (5) showed that the presence of these load cells in the string of rods to the sampler typically produced only a 1% effect on N, and a negligible effect on the magnitude and shape of the first compression wave in the rods.

The writers always placed one such cell as near the hammer as practical and often the second as near the sampler as practical. Refer to these as the

top and bottom cells, respectively, as shown in Fig. 3. The length from the hammer impact point to the top cell Δl_t, varied from approx 2 ft (0.6 m) for the short, donut-shaped hammers to approx 5 ft (1.5 m) for the long safety hammer used in this research. The length between the bottom of the sampler and the bottom load cell Δl_b varied only a few inches from 4 ft (1.3 m). These nonideal cell positions mean one must apply a correction factor, denoted C_η, when using Eq. 6. Instead of the wave traveling a distance $2l$ before its real cutoff, the top load cell shows its apparent cutoff when it has traveled only $2(l - \Delta l_t)$. A reduced distance means a reduced time, which, from Eq. 6, means one would calculate a too low energy content in the first incident compression wave. The same logic applies to the reflected tension wave considered subsequently.

To provide a mathematical basis for the C_η corrections, the writers chose to use the theoretical formula for the wave when $r = 0$, given by Eq. 4. Referring to Eq. 3, when $r \neq 0$ the waves have a mathematically awkward stepped shape. But, over the practical SPT range of $r = 0.02$–$r = 0.15$, they do not differ greatly from that when $r = 0$, and the writers assumed the $r = 0$ solution applies to all r. The writers (11 and 15) both have presented this solution for C_η in convenient graphical form. The writers corrected all energy data presented herein in accord with the preceding procedure.

Energy Reaching Sampler = ENTHRU = E_i.—Herein the symbol E_i denotes the ENTHRU, a term first used by Housel (7) to describe the energy successfully passing through the pile hammer-cushion-anvil system and entering the pile as a compression wave. The E_i = ENTHRU in the SPT represents that part of the E^* = 4,200 in.-lb (474 J) potential hammer energy that successfully reaches the sampler in the form of the initial compression wave. As considered subsequently, wave energy losses during travel through the rods appear negligible. Thus, using Eq. 6 and integrating the force-time wave form obtained from the top load cell in Fig. 3, from the time of hammer impact to the tension cutoff shown in Fig. 1, and after correction for the position of the load cell, should produce the E_i = ENTHRU. This E_i includes all the dynamic energy extracted from the hammer. The ratio E_i/E^* equals the ENTHRU efficiency η with which the SPT system delivers energy to the sampler.

The second writer (11) first measured E_i from over 150 SPT blows using oscilloscope data from the top load cell. After taking photos of the oscilloscope dynamic force versus time ($F' - t$) wave form display, he digitized the wave form using hand methods and eight points per millisecond. He then used a computer to obtain the uncorrected E_i values in accord with Eq. 6, and finally applied the usually small C_η correction to obtain the correct E_i values. The points in Fig. 2 present some of his results in the form of the η efficiency. The 59 blows shown gave η varying from 0.44 to 0.68, which matched well with the previous 0.40 to 0.70 efficiencies reported by Kovacs, et al. (9) for the kinetic energy in the safety hammer at impact when also using two wraps of rope around the cathead.

Since then, the first writer and his assistants have measured η for over 500 SPT blows using a variety of drillrigs and hammers and have found each system's average $\bar{\eta}$ to vary from approx 0.30 to 0.85. The technique for energy calculation first progressed to automatic digitizing of the F'-t wave form and finally to the use of an instrument made by Binary Instruments, Wellesley, Mass., that

displays η immediately after each hammer blow.

N Varies Inversely with E_i.—The first writer (14) presented evidence indicating that N varied inversely with the E' quasi-static energy for SPT sampling—at least to $N = 20$. The writers will now show that the available evidence from dynamic tests also indicates that N varies inversely with E_i to N equal at least 50. As expected, ENTHRU controls N.

Rather than the ordinary N blow count over the ordinary 12-in. (300-mm) SPT sampling interval, the writers report mostly a point value of N in the figures herein, denoted N'. The value N' = the net sampler penetration under a test hammer blow = ΔL divided into 12 in. (300 mm). The value N' equals N only for the condition that the length of sampler penetration into the bottom of the borehole L has the median value of $L = 12$ in. (300 mm) during the blow under investigation. With $L < 12$ in. (300 mm) N will exceed N' somewhat and with $L > 12$ in. N' will exceed N somewhat. This research involved all

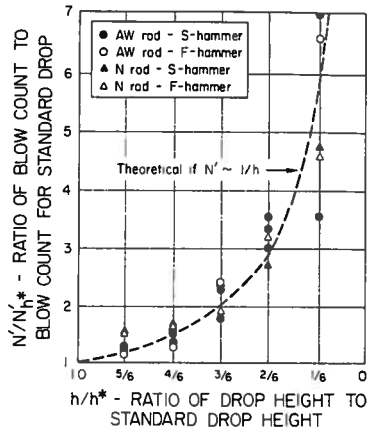

FIG. 4.—Normalized Comparison between Blow Count and Hammer Drop Height

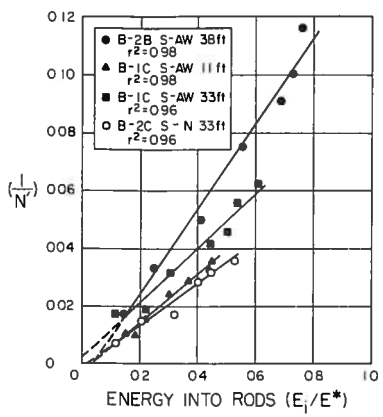

FIG. 5.—Four Series of Reduced Hammer Drop Height Tests Demonstrating Inverse Linear Relationship between Wave Energy and Blow Count

values of L between 6 in. and 18 in. (150 mm and 450 mm) and the writers assumed that any differences between N and N' would average out and considered them equal. They did not correct individual N' data for the effect of L.

Published ENTHRU measurements by the second writer (Ref. 11, Figs. 6.1–6.3) and the first writer (Ref. 15, Fig. 18), as well as many unpublished measurements, have shown that E_i varies approximately linearly with the height of hammer drop h. By performing SPT using hammer drop heights less than the nominal h^* = 30 in. (760 mm), the writers could increase N' and thus could investigate the effect of ENTHRU on N'. Fig. 4 presents the normalized results from five series of such reduced-h SPT blows, involving four hammer-rod combinations.

If N' varied inversely with ENTHRU, and ENTHRU varied directly with the height of hammer drop, then one would predict the hyperbolic relationship between N'/N'_{h^*} and h/h^* shown in Fig. 4 by the dashed line. The data follow

this line and thus support the conclusion that $N \sim 1/E_i$.

Fig. 5 offers more direct data showing that $N' \sim 1/E_i$. This figure presents the N' and E_i data obtained from four series of reduced-h SPT blows. In each series the least-squares line fits well through the data, with a correlation coefficient of at least 0.96 and passing near the origin.

Fig. 6 demonstrates that differences in ENTHRU offer a major reason for the well known variability of N values obtained by different SPT drillers and drill rigs testing the same soil. In this example, each of two rigs performed a series of SPT using rotary drilling and drilling mud in boreholes only 12 ft (3.7 m) apart in a research area demonstrated by other tests to have approximately uniform soil conditions. Yet the average N from the five SPT

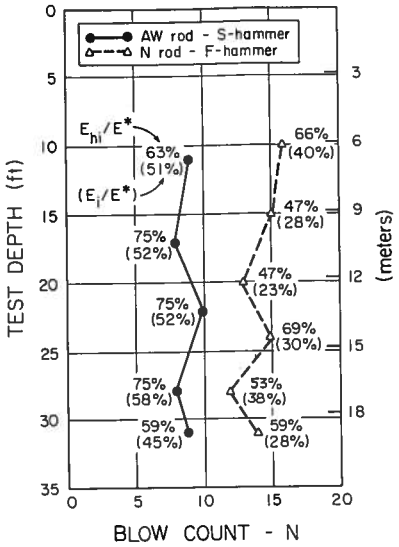

FIG. 6.—Adjacent SPT Data Showing SPT Variability and that ENTHRU Hammer Energy Entering Rods (E_i) Determines N Rather than Energy in Hammer at Impact (E_{hi})

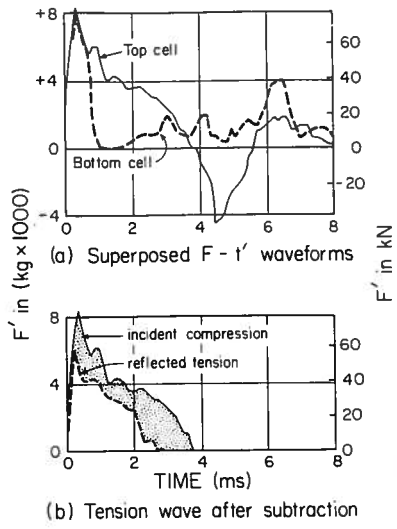

FIG. 7.—Example Data from Top and Bottom Load Cells and Subtraction to Obtain First Reflected Tension Wave (from Ref. 11 Blow No. 51)

in the low-N boring = 8.8, while the average from the six SPT in the high-N boring = 14.2, for an inverse ratio of $(8.8/14.2)^{-1} = 1.61$.

Fig. 6 includes the ENTHRU values measured for each blow. Again using averages, the ratio of E_i/E^* ENTHRU efficiencies = 0.516/0.312 = 1.65. This checks well with the previous inverse-N ratio of 1.61 and helps confirm the inverse relationship between N and ENTHRU and helps explain much of the variability in N values.

Fig. 6 also helps show that the energy in the hammer at impact E_{hi} does not control N because it may not reach the sampler. This figure includes the writers' estimate of each blow's E_{hi}. The second writer (Ref. 11, Figs. 5.18–5.20) had previously demonstrated that the maximum rod stress in the first compression

wave matched well with the predictions of Eq. 2 but at a somewhat reduced level due to impact energy losses. The writers put the measured maximum wave-front stress in the rods into Eq. 2 to obtain the V_{hi} velocity of the hammer at impact. Then $E_{hi} = 0.5$ m $(V_{hi})^2$. Comparing the average E_{hi} values from the borings gives 0.694/0.568 = 1.22, which goes only part way to explain the inverse N ratio of 1.61. For the low-N boring, comparing 0.694 with 0.516 shows an average of at least 26% of the delivered hammer energy, and 18% of E^*, lost in the impact system. For the high-N boring a similar comparison of 0.568 with 0.312 indicates a larger 45% and 26% lost at impact. This example shows that one cannot neglect the energy losses occuring in the impact system. As seems logical, only the ENTHRU can produce the sampler penetration that determines the N value.

Energy in Reflected Wave E_r and Lost to Sampler E_{s1}.—At any point on the rods, at any instant of time, the stress or force in the rods has the value of the instantaneous sum of all incident and reflected waves reaching that point at that time. The top cell provides a force-time (F'-t) record of the first compression wave, but only until its cutoff by the reflected tension wave shortly before t_4 in Fig. 3. Shortly after t_2 the bottom cell provides a force-time record of the subtraction of the reflected tension wave from the incident compression wave. By subtracting the bottom cell force-time record from that of the top cell, Eq. 8 shows that one obtains the reflected tension wave as the difference

$$(F'\text{-}t)_C - [(F'\text{-}t)_C - (F'\text{-}t)_T] = (F'\text{-}t)_T \quad \ldots\ldots\ldots\ldots\ldots\ldots\ldots\ldots (8)$$

One can now use Eq. 6 with the force-time record from the top load cell to compute the incident compression wave energy entering the top of the string of sampling rods E_i. After making the Eq. 8 subtraction, one can use the same equation to get the energy in the reflected tension wave E_r. Then, as stated in Eq. 9, by subtracting these two energies one obtains the energy lost to the sampler during the first reflection of the wave pulse around the sampler

$$E_{s1} = E_i - E_r \quad \ldots\ldots\ldots\ldots\ldots\ldots\ldots\ldots\ldots\ldots\ldots\ldots\ldots\ldots\ldots\ldots (9)$$

Fig. 7 shows an example of applying the preceding methods to an actual SPT blow, No. 51 with $N = 8$, from the second writer (11). Fig. 7(a) shows the superposed force-time records obtained from the top and bottom load cells, taken from oscilloscope photos and incorporating the time correction for the wave to travel from the top to the bottom cell. Fig. 7(b) shows the tension wave obtained by subtraction and compared to the first compression wave. The difference, shaded in both Figs. 3 and 7, represents a measure of the energy E_{s1} given up to the sampler during this reflection of the first wave around the sampler. In this case, $E_i = 0.52\ E^*$ and $E_{s1} = 0.21\ E^* = 0.40\ E_i$.

That portion of the ENTHRU given up to the sampler goes to advance the sampler through the soil at the bottom of the borehole and provides the energy for the "quake" radiating through the soil and away from the sampler. But two extreme soil-strength conditions exist when the sampler cannot accept any of the ENTHRU. With zero resistance to penetration, the perfectly free-ended sampler would reflect all the arriving compression wave as an identical tension wave with the same energy; thus $E_{s1} = 0$. With infinite soil resistance and perfect end-sampler fixity the wave reflects as the identical compression wave,

and again $E_{s1} = 0$. Between these two boundary conditions E_{s1} must first increase as resistance to sampler penetration and therefore N' increases. Eventually, at very high N', E_{s1} must again decrease.

Fig. 8 presents the available data on the variation of N' with the E_{s1}/E_i ratio. The second writer (11) calculated E_{s1} for 138 SPT blows wherein he judged he had good F'-t data from both the top and bottom load cells. Of these, 35 involved hammer drops of less than h^*. All these data came from seven SPT borings, involving three hammer and three rod types but with the majority of the data from when using AW rods and the safety hammer.

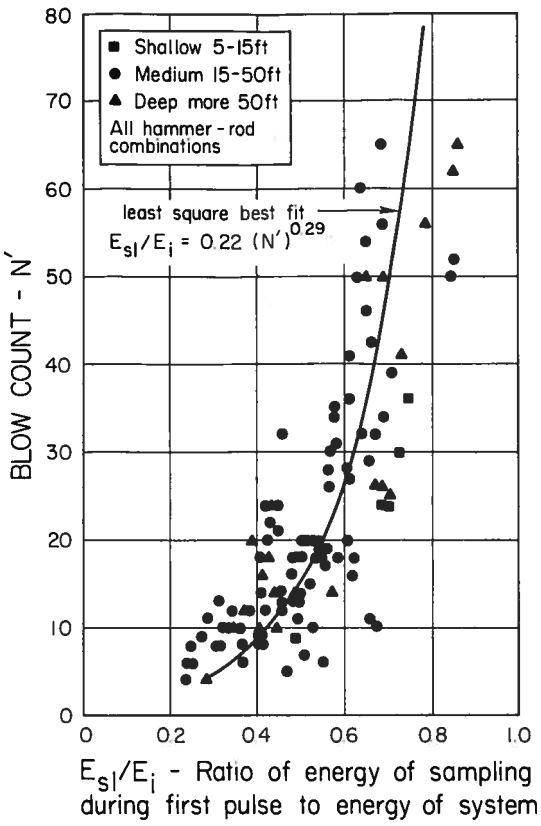

FIG. 8.—Blow Count as Function of Proportion of Wave Energy Lost at Sampler During Reflection of First Wave

Fig. 8 shows the expected increase in E_{s1}/E_i as N' increases. The least squares best fit power curve shows this ratio increasing from approx 0.30 at the relatively low restraint indicated by $N' = 5$, to approx 0.75 at the relatively much higher restraint indicated by $N' = 65$. These data check the aforementioned theory. All the F'-t data showed a reflected tension wave. The writers do not know how high N' must go before the increasing fixity causes a reflected compression wave.

Note also that the legend in Fig. 8 indicates data points with three categories of length l. The intermingling of these data indicate that the relationship shown does not depend on rod length. This seems reasonable from theory because what happens at the sampler end of the rods depends only on the boundary conditions at the sampler-soil interface and not on the length of rods.

The second writer (Ref. 11, Fig. 7.2) also compared the dynamic E_{s1} sampling energy with the E' quasi-static energy required for the same sampler penetration as produced by the hammer blow. Each of the seven SPT borings mentioned previously had at least three Cone Penetration Tests (CPT) surrounding it, and he determined E' by the method presented in Ref. 14. Because of only soil viscosity effects and the radiation loss of dynamic energy in the ground quake, the writers would expect E_{s1} to exceed E'. But the energy lost to the sampler during the first wave reflection cannot exceed that lost during the possibly more than one reflection occurring during the time interval to achieve the full set of the sampler. This effect alone would cause $E_{s1} < E'$. It appears in the 65 available tests with E' evaluations that these effects compensate. The ratio of E_{s1}/E' averages approx 1.06 and appears insensitive to, and possibly independent of, blow count.

Wave Equation Studies

Previous studies by Adam (1) and McLean, et al. (10) showed that the one-dimensional wave equation, ordinarily used to study pile-driving problems, could also model the SPT. These authors did not have the opportunity to validate their computer models with actual q-s E' and SPT F'-t data. Gallet (5) did, and he attempted to duplicate four of the h^* SPT blows recorded by the second writer (11). He used an existing Texas A&M computer program intended for pile studies but which had the capability of also considering the hammer as an elastic body. Lines 1–7 in Table 1 give some of the details of the four blows considered by Gallet.

Gallet placed a load cell in his modeled rod system at approximately the same position as the real top load cell. Lines 8–13 in Table 1 compare some key points in the actual first F'-t wave with the similar points as computed from Gallet's wave equation simulations. Consider also the closeness of the measured and wave equation hammer energies at impact (line 14), and the good agreement in blow count N' (line 15) over the range $N' = 5$–24. There seems little doubt that Gallet's computer models adequately included the key parameters affecting the real SPT dynamic behavior. After thus validating the wave equation model, it and the computer provided a means for studying the SPT with a detail presently not practical with only field measurements.

Hanskat (6) subsequently also made a wave-equation study similar to that by Gallet, but matched 10 real SPT blows instead of four. He also modified the computer program to include the effects of tension slack in the rod joints, damping energy losses in the rods, and to permit the separate modeling of the relatively short, "donut" hammers (B and F hammers herein) and the longer safety hammer (S hammer herein).

Pulsed Sampler Penetration.—Gallet demonstrated that SPT sampler set does not occur with a smooth penetration-time curve. No dynamic penetration occurs until the first compression wave reaches the bottom of the sampler, at time

from impact of approx $0.5t_2$ in the illustration in Table 1. After an initial rapid acceleration to a maximum sampler velocity of about 14 fps (4 m/s) the sampler velocity steadily diminishes until the next cycle arrival of compression pulse, at about time $1.5t_2$. Then, sampler velocity again surges followed by

TABLE 1.—Details of Four SPT Blows Measured by First Writer (11) Versus Model with Wave Equation by Gallet (6).

Palacios blow No.		6		16		18		28		line
Boring, depth (ft)		B-2B, 35		B-3B, 11		B-3B, 22		B-4B, 38		1
Rods + sampler, ℓ (ft)		40		15		28		43		2
L (in)		6		6		6		6		3
Type hammer		Mobile safety		Sprague, & Henwood				donut		4
		(for wave eqn. analyses assumed A_h = 48 in^2 for all)								
Type rods		AW		AW		AW		AW		5
SPT sampler		Assumed 2' long, 1.5" ID, no liners used								6
Type soil		clay		sand		sandy-clay		clay		7
		MEAS.	W. EQN	MEAS.	W. EQN	MEAS.	W. EQN	MEAS.	W. EQN	
FIRST WAVE @ TOP CELL	F'_1 (lb)	20675	21250	16200	15900	19000	18750	19000	18750	8
	t_1 (ms)	0.7	0.8	0.65	0.75	0.6	0.75	0.6	0.8	9
	F'_2	4410	4190	8150	7930	7930	6390	3525	2975	10
	t_2	5.0	4.6	2.0	1.9	3.3	3.2	5.4	4.9	11
	F'_3	-12125	-9920	-6610	-5070	-6830	-6830	-7710	-7710	12
	t_3	6.0	5.2	2.8	2.3	4.2	3.85	6.3	5.5	13
E_{hi}/E^*			69%		39%		53%		53%	14
E_i (eqn 6) $/E^* = n$		63%		38%		60%		60%		15
N' = 305mm/ΔL		5	5.5	19	19.1	24	23.2	9	9.2	16
QUASI-STATIC FORCES ON SAMPLER (lb) (from parallel CPTs - see Ref (12))	F_e		330		1403		1415		465	17
	$F_i + F_o$		157		402		487		204	18
	F + W'		487		1805		1902		669	19
	- W'		-187		-78		-130		-195	20
	F		304		1727		1772		474	21
	F/nN	140		283		153		123		22
FOR SAMPLER PEN. TO 90% ΔL	No. wave cycles		8		9		3		5	23
	Δt (ms)		38		15		8		27	24
	$\bar{V}_s$ (ft/s)		4.2		3.2		4.5		3.7	25
	max V_s "								14.6	26
DAMPING FACTORS	J_p (s/ft)		0.36		0.09		0.26		0.36	27
	J_s "		0.12		0.03		0.05		0.12	28
AVE DYNAMIC FORCES ON SAMPLER (lb)	$\bar{F}_{ed}$		829		1807		3071		1084	29
	$\bar{F}_{sd}$		236		470		597		295	30
	$\bar{F}_d$ + W'		1065		2277		3668		1379	31
	$\bar{F}_d$		882		2199		3538		1184	32
	$(\bar{F}_d/F)$		2.9		1.3		2.0		2.5	33
% ΔL, 1st wave cycle			24%		32%		50%		28%	34

1 ft = 305mm 1 in. = 25.4 mm 1 lb = 4.45 N

gradual decay until the next-cycle surge at $2.5t_2$, etc. Fig. 9 shows this process with some of Hanskat's computer results from blow 28.

Fig. 9(*a*) shows the contact force between the hammer and the top of the rods versus time from hammer impact. This closely represents the F'-t wave

form of the first compression wave that travels down the rods to the sampler. The points "1" and "2" shown match those shown in the Table 1 example, and they come from the top load cell data from blow 28. Note that at 5.0 msec, which equals $2l/c$ for blow 28, the contact force drops to zero and remains at zero because the rods have pulled away from the still-falling hammer. Eventually the hammer will again strike the rods, but the computer study shows it will then have a kinetic energy content of only about $0.04E^*$, compared to its initial $0.60E^*$ and cannot produce significant additional penetration of the sampler.

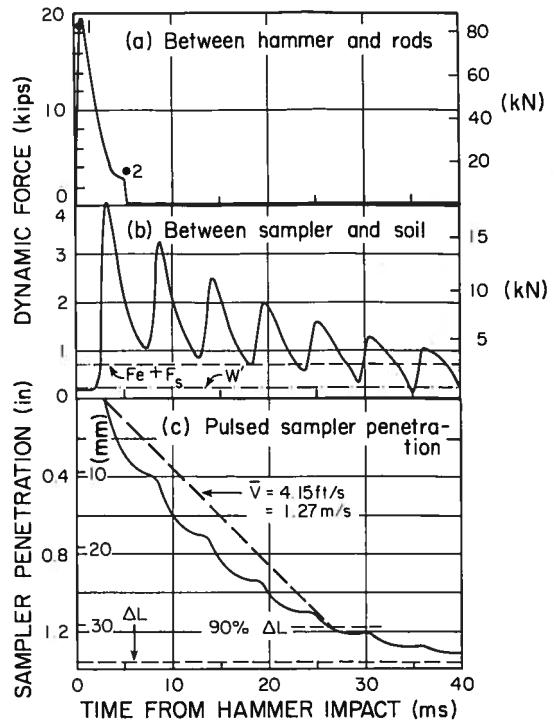

FIG. 9.—Hanskat's (6) Wave Equation Model Results from Simulated Blow No. 28 of Ref. 11 Showing Hammer Cutoff and Pulsed Soil Sampler Forces and Penetration

Fig. 9(*b*) shows, to an expanded force scale, the total dynamic force between the sampler and the soil F_d versus time from hammer impact. For reference, this figure also shows the q-s resistance to sampler penetration and the W' weight of only the rods. One can see that the SPT applies a decaying series of F_d-t pulses synchronous with the wave traverses up and down the rods and that F_d varies greatly during the total time required for sampler penetration.

Fig. 9(*c*) shows the pulses of sampler penetration that occur in response to the pulses in dynamic penetration force shown in Fig. 9(*b*). Because each pulse has a successively reduced energy content each produces a reduced increment of penetration compared to the previous increment. In this Hanskat

model, the first pulse produced 31% of the final penetration and it took five wave cycles and 26 msec from impact to achieve 90% penetration. For blow 28, the experimental $E_{s1}/E_i = 28\%$, which matches well with the preceding 31% and suggests that most of E_{s1} goes to produce sampler penetration.

Table 1, line 23, gives the number of wave cycles required to achieve 90% of the final set resulting from each blow. Line 34 shows the percentage of penetration during the first pulse, from Gallet's study. Hanskat used a slightly different model and obtained slightly different results. However, both showed that the number of cycles decreased, and the percentage of penetration during the first pulse increased, as either N or l increased.

The frequency of the sampling pulses depends on l and the effective c. Eq. 10 gives the approximate frequency f_p, i.e.

$$f_p\,(\text{Hz}) = \frac{8{,}000}{l}\,(\text{ft}) \quad \text{(10)}$$

Sampling Time and Velocities.—The short horizontal line on the curve in Fig. 9(*c*) marks the point of 90% set. The time difference between the time from impact at this 90% point and the arrival at the sampler of the first wave pulse, $0.5t_2$, denoted Δt_{90}, represents the time of sampler penetration to 90% set. Table 1, line 24, notes this time for Gallet's four blows, in milliseconds.

Fig. 10 presents a graph of N' versus the preceding time interval and also the 50% set times, with Gallet's four and Hanskat's 10 blows plotted. Recognizing that $N' = \infty$ means no penetration, which would require 0 time, and $N' = 0$ means continuous penetration under self weight, which would require infinite time, the writers then estimated approximate hyperbolic curves through the data. Eq. 11 fits the 90% data:

$$\Delta t_{90}\,(\text{ms}) = \frac{200}{N'} \quad \text{(11)}$$

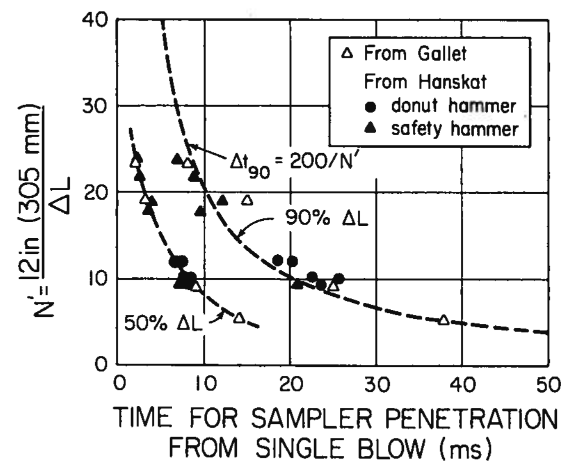

FIG. 10.—Wave Equation Model Results Showing Inverse Relationship between Blow Count and Time for Sampler Penetration from Single Blow

The writers also estimated the average sampler velocities during the first 90% of set as the secant slope from 0%–90%, as shown in Fig. 9. Table 1, line 25, lists these estimates. Note the rather narrow range from Gallet of 3.2 fps–4.5 fps, (0.98 m/s–1.4 m/s), despite the N' range of 5.5–23.5. The computer data for time penetration show that the sampler penetrates at about the same initial velocity for all blows—12 fps–15 fps (3.7 m/s–4.6 m/s). Average velocities at 90% set all equal about 1.5 fps (0.46 m/s). It thus appears that initial, final, and average sampler penetration velocities remain approximately independent of N'. A constant average penetration velocity would mean $\Delta t_{90} \sim 1/N'$, which checks with Eq. 11.

Dynamic Soil Resistance.—The availability of parallel CPT data permitted Gallet and Hanskat to estimate the q-s F_e and $F_i + F_o$ soil resistance forces acting on the sampler during each blow. Lines 17 through 21 in Table 1 list Gallet's forces and the net q-s F, but the sampler has to overcome dynamic soil resistance. The wave equation program determines dynamic forces by using Eqs. 12 for end and side resistances

$$F_{ed} = F_e(1 + J_p V_s) \quad \text{(12a)}$$

$$F_{sd} = (F_i + F_o)(1 + J_s V_s) \quad \text{(12b)}$$

in which F_{ed} = dynamic sampler end resistance; F_{sd} = dynamic sampler side resistance; J_p = end "damping factor"; J_s = side "damping factor"; and V_s = velocity of bottom end of sampler. After matching wave form and energy by manipulating other factors, Gallet matched N' by varying J_p and J_s. Lines 27 and 28 present his final values, which fall within the ranges often used in pile-driving problems. Using these J values, the q-s resistances in Table 1 and the average sampler velocities listed on line 25 the writers obtained the average dynamic soil resistances shown in lines 29 through 32. However, Fig. 9(*b*) shows that F_d varies greatly during penetration and an average $\bar{F}_d$ represents a great simplification.

Note that the SPT appears to provide data, which when analyzed by the wave equation can produce site-specific J_p and J_s values for practical pile-driving studies.

Negligible Energy Losses in Rods.—Many engineers have wondered about the extent of energy losses in the rods during the first and subsequent excursions of the compression wave resulting from hammer impact. To reduce such losses, as from lateral rod "whipping," engineers often require stiffer rods such as N-rod rather than A-rod. The previous wave equation studies by Adam (1) and McLean, et al. (10) indicated that the type of rod should have only a negligible effect on N values. These studies could not include possible whipping. However, a recent field comparison study by Brown (2) to depths of 110 ft (34 m) indicated that A-rod versus N-rod had no measurable effect on N values. The new research considered in this paper also suggests that any whipping or other effects have a negligible effect on wave energy transmission to the sampler to depths of at least 70 ft (21 m), as does the type of rod used.

The second writer (11) and Smith (16) made many comparisons of the first compression F'-t wave as measured by the top and bottom load cells. They found from random blow selections that the maximum F' and the form of the head of the wave to the tension cutoff at the bottom cell did not differ

significantly at the 95% confidence level. Fig. 7(*a*) shows an example.

Hanskat (6) included varying levels of steel material damping energy losses in the rods as a method of simulating rod energy losses, and matched the resulting wave forms with the real data. He concluded that such energy losses appeared negligible. He also included varying slack at the rod joints but found this had only a very small effect on N values. This checked a previous similar conclusion by Adam (1).

All the field and computer simulation data available indicate that the type of rod used and the tightness of the joints have a very minor effect on N and that almost all of E_i gets to the sampler.

Type of Hammer.—McLean, et al. (10) modeled two types of the relatively short, donut hammers that strike at their bottom faces and produce an initial compression wave in the hammer. They found a negligible difference in the N value results. Hanskat (6) also modeled two hammers, one the donut shape where he used five elements, each 2.5 in. (63 mm) long, and the other the much longer safety hammer, where he used eight elements, each 6 in. (152 mm) long, which has an internal anvil at its top and produces an initial tension wave in the hammer. He found that with V_{hi} equal, both hammers produced very similar wave forms and N values.

It appears from these studies that the type of hammer used, at least within the ordinary range of geometries for SPT 140 lb (620 N) hammers, has a negligible effect on N. Note that this does not apply to the hammer drop system, nor to the anvil or cushion system, either of which might greatly affect ENTHRU and therefore N.

Practical Applications

This paper, together with Ref. 14, should end the common perception of the SPT as a purely empirical in-situ test. They include many theoretical and practical insights into the mechanics of the SPT sampling process with quantitative information about the forces, energies, and times involved in SPT sampling and N values.

The evidence herein provides a further, very strong, demonstration that N values vary inversely with the hammer-induced dynamic compression wave energy reaching the sampler—the ENTHRU, denoted E_i. The writers also provide some data to demonstrate the great variability in E_i in current United States' practice and thus in N values in the same soil. Any standardization of the SPT aimed at reducing variability in N values must include standardizing E_i or correcting N values to a standard E_i. This paper describes a practical method for measuring E_i to help accomplish this objective.

The apparent fact that each SPT blow loads the sampled soil in cyclic undrained shear lends practical support to the use of N values as an index test for liquefaction potential. The SPT also offers engineers a model of pile driving. As demonstrated herein, appropriate analysis of SPT data can lead to site-specific J damping coefficient values for use with the one-dimensional wave equation computer model of a pile-driving problem.

Conclusions

The writers have presented a theoretical, experimental, and computer study

of the force and energy dynamics of the SPT sampler penetration. Their conclusions include:

1. The theory presented appears to successfully predict the experimental SPT data observed in this study.
2. This paper describes a successful method for using a single, force-time load cell below the hammer to measure the ENTHRU portion of the hammer energy that actually enters the rods.
3. The evidence presented herein strongly supports that N varies inversely with ENTHRU to at least $N = 50$. Most of ENTHRU goes into pushing the sampler into the soil.
4. To at least $N = 50$, the first impact of the hammer provides all the ENTHRU useful to sampling. The rods first separate from the hammer at time $2l/c$ after impact.
5. Measurements of ENTHRU from over 500 SPT blows from a variety of drill rigs and hammers have shown that it can vary from 30%–85% of the free-fall hammer energy. This implies that N could vary by a factor of almost three in the same soil due to only variable ENTHRU.
6. A variety of evidence indicates that the type of rods, from A-rod to NW-rod for depths to 110 ft (34 m), and the tightness of the rod joints, have a negligible effect on ENTHRU and on N values.
7. The type of hammer has a negligible effect on N values provided ENTHRU remains the same.

Acknowledgments

The Florida Department of Transportation, under the project direction of Robert Ho, and the University of Florida Engineering and Industrial Experiment Station sponsored the research described in this paper. William J. Whitehead, Assistant in Engineering with the University of Florida Department of Civil Engineering, helped perform much of the associated field work.

Appendix.—References

1. Adam, J., discussion of "The Standard Penetration Test," by V. F. B. deMello, *Proceedings*, Fourth PanAmerican Conference on Soil Mechanics and Foundation Engineering, Vol. III, 1971, pp. 82–84.
2. Brown, R. E., "Drill Rod Influence on Standard Penetration Test," *Journal of the Geotechnical Division*, ASCE, Vol. 103, No. GT11, Proc. Paper 13313, Nov., 1977, pp. 1332–1336.
3. Fairhurst, C., "Wave Mechanics of Percussive Drilling," *Mine & Quarry Engineering*, Mar., 1961, pp. 122–130, Apr., 1961, pp. 169–178, July, 1961, pp. 327–328.
4. Fisher, H. C., "On Logitudinal Impact. Fundamental Cases of One-Dimensional Elastic Impact. Theories and Experiments," *Applied Science Research*, Section 8, Vol. 8, 1960.
5. Gallet, A. J., "Use of the Wave Equation to Investigate Standard Penetration Test Field Measurements," thesis presented to the University of Florida, at Gainesville, Fla., in 1976, in partial fulfillment of the requirements for the degree of Master of Engineering.
6. Hanskat, C. S., "Wave Equation Simulation of the Standard Penetration Test," thesis presented to the University of Florida, at Gainesville, Fla., in 1978, in partial fulfillment of the requirements for the degree Master of Engineering.

7. Housel, W., "Michigan Study of Pile Driving Hammers," *Journal of the Soil Mechanics and Foundations Division*, ASCE, Vol. 91, No. SM5, Proc. Paper 4483, Sept., 1965, pp. 37–64.
8. Kolsky, H., *Stress Waves in Solids*, Oxford University Press, Oxford, England, 1951.
9. Kovacs, W. D., Evans, J. C., and Griffith, A. H., "Towards a More Standardized SPT," *Proceedings*, Ninth International Conference on Soil Mechanics and Foundation Engineering, Vol. 2, pp. 269–276, 1977.
10. McLean, F. G., Franklin, A. G., and Dahlstrand, T. K., "Influence of Mechanical Variables on the SPT," *Specialty Conference on the In Situ Measurement of Soil Properties*, ASCE, Vol. 1, 1975, pp. 287–318.
11. Palacios, A., "The Theory and Measurement of Energy Transfer During Standard Penetration Test Sampling," thesis presented to the University of Florida, at Gainesville, Fla., in 1977, in partial fulfillment of the requirements for the degree of Doctor of Philosophy.
12. Schmertmann, J., discussion of "The Standard Penetration Test," by V. F. B. deMello, *Proceedings*, Fourth PanAmerican Conference on Soil Mechanics and Foundation Engineering, Vol. III, 1971, pp. 90–98.
13. Schmertmann, J., "Use the SPT to Measure Dynamic Soil Properties?—Yes, But . . .!," *Dynamic Geotechnical Testing*, ASTM STP 654, American Society for Testing and Materials, 1978, pp. 341–355.
14. Schmertmann, J., "Statics of SPT," *Journal of the Geotechnical Division*, ASCE, Vol. 105, No. GT5, Proc. Paper 14573, May, 1979, pp. 655–670.
15. Schmertmann, J., "The Statics and Dynamics of the Standard Penetration Test," *Proceedings*, Federal Highway Administration Symposium on Site Exploration in Soft Ground Using In-Situ Techniques, May, 1978 (in press).
16. Smith, T. V., "A Summary of Energy Calibration Tests on SPT Equipment," thesis presented to the University of Florida, at Gainesville, Fla., in 1977, in partial fulfillment of the requirements for the degree of Master of Engineering; see also *Geotechnical Testing Journal*, American Society for Testing and Materials, Vol. 1, No. 1, Jan., 1978, p. 57.

14769 ENERGY DYNAMICS OF SPT

KEY WORDS: **Drilling;** Energy; **Field tests; Soil dynamics;** Soil mechanics; **Soil sampling; Standard penetration tests;** Theory; Wave equations

ABSTRACT: The writers report on the dynamics of the standard penetration test (SPT) as determined from a study involving hammer impact and wave mechanics theory, field measurements of dynamic behavior during SPT, and computer simulations using the wave equation as developed for computer studies of pile driving. The field data match well with the theory presented and the simulations provided further insight into the details of SPT sampler penetration. The work includes methods for determining the amount of hammer enery reaching the sampler, and for determining the energy lost to the sampler. The writers conclude that blow count varies inversely with the wave energy reaching the sampler, and that the SPT represents a form of in situ, undrained, cyclic load test and offers a method for site-specific determinations of the J damping coefficients in wave equation analyses of pile driving.

REFERENCE: Schmertmann, John H., and Palacios, Alejandro, "Energy Dynamics of SPT," *Journal of the Geotechnical Engineering Division,* ASCE, Vol. 105, No. GT8, **Proc. Paper 14769**, August, 1979, pp. 909-926